CHEMISTRY
A EUROPEAN JOURNAL

ChemPubSoc
Europe

DOI: 10.1002/chem.201204070

Fluorinated Carbohydrates as Lectin Ligands: Dissecting Glycan–Cyanovirin Interactions by Using ^{19}F NMR Spectroscopy

Elena Matei,[a] Sabine André,[b] Anja Glinschert,[c] Angela Simona Infantino,[c] Stefan Oscarson,[c] Hans-Joachim Gabius,[b] and Angela M. Gronenborn*[a]

Abstract: NMR spectroscopy and isothermal titration calorimetry (ITC) are powerful methods to investigate ligand–protein interactions. Here, we present a versatile and sensitive fluorine NMR spectroscopic approach that exploits the ^{19}F nucleus of ^{19}F-labeled carbohydrates as a sensor to study glycan binding to lectins. Our approach is illustrated with the 11 kDa Cyanovirin-N, a mannose binding anti-HIV lectin. Two fluoro-deoxy sugar derivatives, methyl 2-deoxy-2-fluoro-α-D-mannopyranosyl-(1→2)-α-D-mannopyranoside and methyl 2-deoxy-2-fluoro-α-D-mannopyranosyl-(1→2)-α-D-mannopyranosyl-(1→2)-α-D-mannopyranoside were utilized. Binding was studied by ^{19}F NMR spectroscopy of the ligand and ^{1}H–^{15}N HSQC NMR spectroscopy of the protein. The NMR data agree well with those obtained from the equivalent reciprocal and direct ITC titrations. Our study shows that the strategic design of fluorinated ligands and fluorine NMR spectroscopy for ligand screening holds great promise for easy and fast identification of glycan binding, as well as for their use in reporting structural and/or electronic perturbations that ensue upon interaction with a cognate lectin.

Keywords: fluorine · fluoro-deoxy sugars · lectins · ^{19}F NMR spectroscopy · protein–ligand interactions · titration

Introduction

The growing realization of the enormous potential of glycans in information coding, embodied by the term "sugar code",[1] has led to define oligosaccharides as functionally active units and provides the rational for identifying new targets in drug design. Aided by the advances in chemical synthesis of such determinants,[2] the detection of glycan receptors (lectins) and the analyses of the specificity/mechanisms of protein–carbohydrate interactions are key steps in this endeavor.[3] With glycan-receptor recognition critically involved in viral and bacterial cell attachment, as well as in host defense, immune(dys)regulation and tumor progression,[4–8] versatile and sensitive analysis/screening tools in this area are urgently needed. NMR spectroscopy can satisfy this need, having proved its value by providing high-resolution molecular structures in solution and valuable information on ligand binding.[9–12]

Most biomolecular NMR applications employ proton/carbon/nitrogen experiments and 2D heteronuclear NMR spectroscopy is a powerful method to map ligand binding sites on proteins and to quantify protein–ligand interactions.[9–12] It has, however, some limitations. It is best suited for medium size proteins (<50 kDa) since amide resonance assignments are a prerequisite. In addition, for titration experiments with low affinity ligands, large amounts of ligand are needed to reach saturation, introducing uncertainty in the estimation of affinity parameters, especially for synthetic compounds of limited water-solubility. Thus, ligand-centered methods hold some promise to overcome these problems.

Among ligand-detected NMR approaches, only few exploit the favorable properties of the fluorine nucleus.[13,14] Mono- or trifluoro *N*-acetylglucosamines were used to measure affinity constants and map their binding environment.[15–18] By using fluorinated sugars,[19–21] saturation transfer difference (STD) experiments in which magnetization was relayed to the vicinal and geminal F-atoms in a monosaccharide were used in a competition screening assay in the search for lead compounds in inhibitor design.[22,23] Analogous to isothermal titration calorimetry (ITC), in which in addition to titrating the ligand into the protein solution, a second, reverse titration can be performed so that the protein is titrated into the ligand solution, ligand-based NMR titrations provide the reciprocal data to information commonly extracted from 2D ^{1}H,^{15}N heteronuclear correlation spectra of the protein. If the correct model is used for data

[a] Dr. E. Matei, Prof. Dr. A. M. Gronenborn
Department of Structural Biology
University of Pittsburgh School of Medicine
Pittsburgh, PA 15260 (USA)
E-mail: amg100@pitt.edu

[b] Dr. S. André, Prof. Dr. H.-J. Gabius
Institute of Physiological Chemistry
Faculty of Veterinary Medicine
Ludwig-Maximilians-University Munich
Veterinärstrasse 13, 80539 Munich (Germany)

[c] Dr. A. Glinschert, A. S. Infantino, Prof. Dr. S. Oscarson
Centre for Synthesis and Chemical Biology
UCD School of Chemistry and Chemical Biology
University College Dublin, Belfield, Dublin 4 (Ireland)

Supporting information for this article is available on the WWW under http://dx.doi.org/10.1002/chem.201204070.

fitting, identical thermodynamic parameters should be obtained, regardless of the direction of the titration.[24]

Here we present a NMR study in which the ^{19}F NMR signal of a singly fluorinated small molecule ligand is monitored upon protein addition. We compare these data to the results obtained by recording changes in ^{1}H,^{15}N amide protein resonance frequencies upon ligand binding. For our study we selected the 11 kDa antiviral lectin cyanovirin-N (CV-N) as the sugar receptor, because its structure and glycan-binding properties have been carefully analyzed by NMR spectroscopy, crystallography, and titration calorimetry.[25–28] CV-N harbors two carbohydrate-binding sites in its pseudo-symmetric, bilobal structure, site 1 in domain B (residues 39–89) and site 2 in domain A (residues 1–38/90–101).[25–28] The minimal glycan recognition unit is a α-1,2-linked dimannoside, either as the individual oligosaccharide or as part of the terminal arms of the branched Man-8 and Man-9 structures.[29,30] Domain A exhibits a slight preference for trimannoside and domain B for dimannoside.[28,31,32] The availability of detailed STD data for these ligands as well as results with specific deoxy sugars allowed us to identify the pivotal hydroxyl groups responsible for binding.[33,34] In particular, we determined that the 3′- and 4′-hydroxyl groups are essential for the interaction, whereas the 2′- and 6′-hydroxyl groups of the Manα(1-2)Manα(Man2) terminal unit are not directly involved in CV-N binding.[34] We therefore prepared methyl 2-deoxy-2-fluoro-α-D-mannopyranosyl-(1→2)-α-D-mannopyranoside (^{19}F-Manα(1-2)Manα, hereafter ^{19}F-Man2) and methyl 2-deoxy-2-fluoro-α-D-mannopyranosyl-(1→2)-α-D-mannopyranosyl-(1→2)-α-D-mannopyranoside (^{19}F-Manα(1-2)Manα(1-2)Manα, hereafter ^{19}F-Man3) (see the Supporting Information, Scheme S1) for use in our current work.

We show that fluorination at the 2′ or 2″ position of the sugar does not curtail its bioactivity in a cell-binding assay in which ^{19}F-Man2 and ^{19}F-Man3 were used as inhibitors for the interaction of CV-N with the cell surface. We determined affinity constants and exchange rates for ^{19}F-Man2 and ^{19}F-Man3 interaction with two of the CV-N variants in which one of the binding sites had been impaired,[35–37] and compared the results to the values derived from titration calorimetry.

In addition, due to the inherent high sensitivity of the fluorine chemical shift to its local environment, it was possible not only to distinguish between free and bound signals for ^{19}F-Man2 and ^{19}F-Man3, but also to identify two different modes of binding for ^{19}F-Man3.

Results and Discussion

NMR spectroscopy is becoming a standard approach for studying protein–ligand interactions because it provides powerful means for mapping the structural details of binding sites on the protein as well as the ligand. In addition, affinity parameters can be determined. Here, we employed ^{19}F NMR spectroscopy and fluorinated ligands to evaluate the interactions between di- and trimannoside with CV-N and demonstrate that, based on the favorable properties of the ^{19}F nucleus, new features can be discerned.

Bioactivity of the ^{19}F-containing glycans: To ascertain that substituting a fluorine at the 2′ or 2″ position for the hydroxyl group does not alter the properties of the sugars significantly and that the two 2′-^{19}F-substituted dimannoside and the 2″-^{19}F-substituted trimannoside are capable to act as specific and potent ligands, we tested their activity in blocking the binding of lectin to cells. As shown in Figure 1, 2′-^{19}F-substituted glycans strongly inhibited the binding of lectin to human carcinoma cells, when compared with the natural monosaccharide. Similar data were also obtained for a T lymphoma (Jurkat) line (not shown).

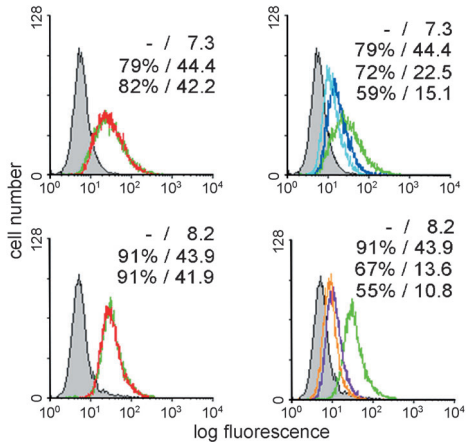

Figure 1. Cell-binding of monofluorinated di- and trimannosides. Human colon adenocarcinoma cells (SW480) were stained with fluorescein-labelled CV-N. Controls representing staining with CV-N (100%-value at 1 μg mL^{-1}; green line) and without (0%-value; shaded area) are included in each panel (quantitative data for the percentage of positive cells/mean fluorescence intensity are listed). Top panel: control experiment without added glycan (green) and in the presence of 100 mM mannoside (left), and in the presence of 4 mM or 8 mM ^{19}F-Man2 (right). Bottom panel: control experiment without added glycan (green) and in the presence of 100 mM mannoside (left), in the presence of 1 mM or 2 mM ^{19}F-Man3 (right).

Therefore, incorporation of the ^{19}F sensor did not impair bioactivity, confirming that the 2′ groups are not critical for cell surface receptor binding on the two cell types tested, which is in line with expectations based on results with the 2′-deoxy derivative of the dimannoside.[34] These results prompted us to proceed in studying the interaction with the lectin by using ^{19}F NMR spectroscopy.

Ligand-detected binding of fluorinated sugars to CV-N: For ligand-detected NMR experiments we recorded the 1D-^{19}F NMR spectra of ^{19}F-Man2 (200 μM) and ^{19}F-Man3 (50 μM) at 280 K. Spectra of 1:1 mixtures of sugar/protein are provided in Figure 2A and 2B for $[CVN^{\Delta A}]_{ssm}$, CVN^{mDB} and CV-N^{P51G} with ^{19}F-Man2 and ^{19}F-Man3, respectively.

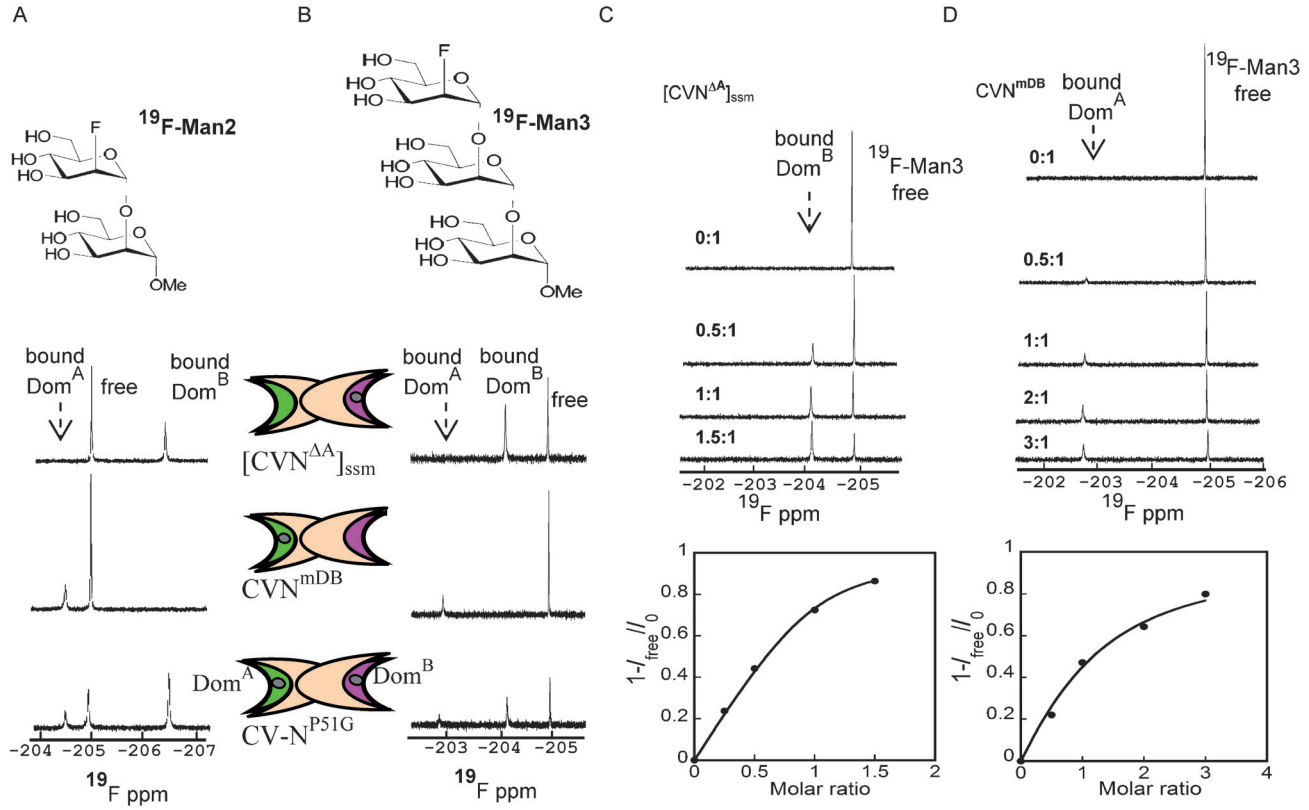

Figure 2. 1D-^{19}F NMR spectra (at 280 K) of ^{19}F-Man2/Man3 in the presence of $[CVN^{\Delta A}]_{ssm}$, a variant that contains a single glycan binding site on domain B, CVN^{mDB}, a variant that contains a single glycan binding site on domain A, and CV-N^{P51G} that is wild-type-like with both glycan binding sites present. CV-N domains are represented by two elongated crescents, representing the two binding sites. Site 1 on domain B is colored pink and site 2 on domain A in green. A) ^{19}F-1D NMR spectra of 200 μM ^{19}F-Man2 in the presence of $[CVN^{\Delta A}]_{ssm}$, CVN^{mDB}, and CV-N^{P51G}; B) ^{19}F-1D NMR spectra of 50 μM ^{19}F-Man3 in the presence of $[CVN^{\Delta A}]_{ssm}$, CVN^{mDB} and CV-N^{P51G}. Bound-state and free-state signals are in slow exchange for $[CVN^{\Delta A}]_{ssm}$ (in C) and CVN^{mDB} (in D). In the titration curves (bottom panels) the bound fraction is derived from the signal intensity ($1-I_{free}/I_0$) during the titration, with I_{free} the intensity of the free ligand signal at each point in the titration, and I_0 is the intensity of the free ligand signal at the beginning of the titration. In C) $[CVN^{\Delta A}]_{ssm}$ was titrated into 50 μM ^{19}F-Man3 (top panel), with molar ratios of protein/glycan: 0:1, 0.5:1, 1:1, 1.5:1. In D) CVN^{mDB} was titrated into 50 μM ^{19}F-Man3 (top panel), with protein/glycan molar ratios: 0:1, 0.5:1, 1:1, 2:1, and 3:1.

Two distinct resonances, separated by a $\Delta\delta > 1$ ppm, correspond to the protein-free and protein-bound conformations. The resonance corresponding to the protein-bound conformation of ^{19}F-Man2 when bound to domain A is shifted downfield from the free resonance, whereas that corresponding to the domain B protein-bound confirmation is shifted upfield. The two resonances of ^{19}F-Man3 when bound to domain A and B both experience a downfield shift, compared with the signal of the free sugar. Unambiguous assignments to the domain A-bound or domain B-bound state was achieved by using $[CVN^{\Delta A}]_{ssm}$ and CVN^{mDB}, variants of CV-N in which the binding site in domains A and B were obliterated.[35–37] Gratifyingly, the two resonances corresponding to bound ^{19}F-Man2 in the CV-N^{P51G} wild-type variant of CV-N that possesses both binding sites, exhibit identical chemical shifts to those observed in the single site mutants, confirming that the site that remains in the mutant is identical to its wild-type counterpart. The same holds for the ^{19}F-Man3 resonances, although as pointed out above, both bound resonances are downfield of the signal of the free sugar.

Much of the power of fluorine NMR studies of biological systems derives from the high sensitivity of the fluorine shielding parameter to changes in local environment. Shielding is observed when the fluorine is in close contact to H-bond donors of the protein or solvent molecules.[38–40] On the contrary, a fluorine nucleus in the vicinity of an electronegative atom shifts downfield. Also, deshielded fluorine atoms are found in close contact with hydrophobic side-chains.[38–40] Inspection of the crystal structure of a mutant CV-N protein, in which the carbohydrate binding site in domain A was abolished, complexed with a dimannoside ligand, P51G-m4-CVN/Man2 (PDB accession code 2RDK),[41] revealed that in the binding site on domain B, a 2′-^{19}F substitution could act as a H-bond acceptor with a vicinal water molecule, causing an upfield shift. Unfortunately, structural data for dimannoside binding in domain A are not available, therefore we can only speculate that such H-bond is not present for 2′-^{19}F-Man2 interacting with domain A. The small ^{19}F downfield chemical shift observed in this case is most likely caused by either anionic repulsion by an electronegative protein atom or an interaction of the fluo-

rine atom with the hydrophobic protein-binding pocket. For Man3, the crystal structures of wild-type CV-N bound to Man9 (PDB accession code 3GXZ)[32] allows to delineate residues in domain A that interact with the trimannoside on the D1 arm of Man9. The negative Glu101 side-chain carboxylate causes electrostatic repulsion of the anionic 2″-^{19}F, resulting in a downfield shift. A similar scenario or possibly contacts with hydrophobic protein side-chains are likely for ^{19}F-Man3 binding to domain B, although direct supporting structural data are not available.

We also carried out 1D-^{19}F NMR experiments at 298 K. However, except for the resonance of the free fluorinated glycan, no signal for the ligand-bound to protein conformation was detected in the case of ^{19}F-Man2, complexed with all CV-N variants. This is probably due to severe line broadening in the intermediate exchange regime at room temperature. For ^{19}F-Man3, on the other hand, both ligand-free and ligand-bound resonances were detected at 298 K when $[CVN^{\Delta A}]_{ssm}$, CVN^{mDB} or CV-N^{P51G} was added, although the ligand-bound resonances were significantly broader than the ones at 280 K (data not shown). The 1D ^{19}F NMR titration data, monitoring the ^{19}F-Man3 resonance intensities upon addition of $[CVN^{\Delta A}]_{ssm}$ and CVN^{mDB} at 280 K, are provided in Figure 2C and 2D, respectively. The spectra for ^{19}F-Man3 (50 μM) are displayed in the top panels and the resulting binding isotherm in the bottom panel. For both mannosides, the free and bound resonances are in slow exchange. The K_D^F values were extracted from the binding isotherms, monitoring the intensity changes of the protein-bound ligand signal versus the protein/ligand molar ratio. The bound fraction (f_b) was estimated from the intensity changes of the free ligand resonance during the titration using $f_b = 1 - I_{free}/I_0$. The extracted K_D^F values were 10.8 ± 0.3 μM for $[CVN^{\Delta A}]_{ssm}$ and 33.5 ± 3.5 μM for CVN^{mutDB} binding to ^{19}F-Man3, respectively.

Exchange kinetics between free and protein-bound fluorinated glycans: The ^{19}F NMR resonances for free and bound states at 280 K are in slow exchange on the chemical shift scale, as evidenced by exchange peaks in the 2D ^{19}F-^{19}F NOESY spectra.

To extract the kinetic parameters for the exchange process, a series of 2D ^{19}F-^{19}F homonuclear NOESY spectra with different mixing times were recorded. Representative spectra of ^{19}F-Man2 (200 μM) in the presence of $[CVN^{\Delta A}]_{ssm}$ and CVN^{mDB} (1:1 molar ratio) at 280 K are provided in Figures 3A and 3B. The exchange curves obtained from the intensity ratios of the bound, diagonal peak, to the exchange

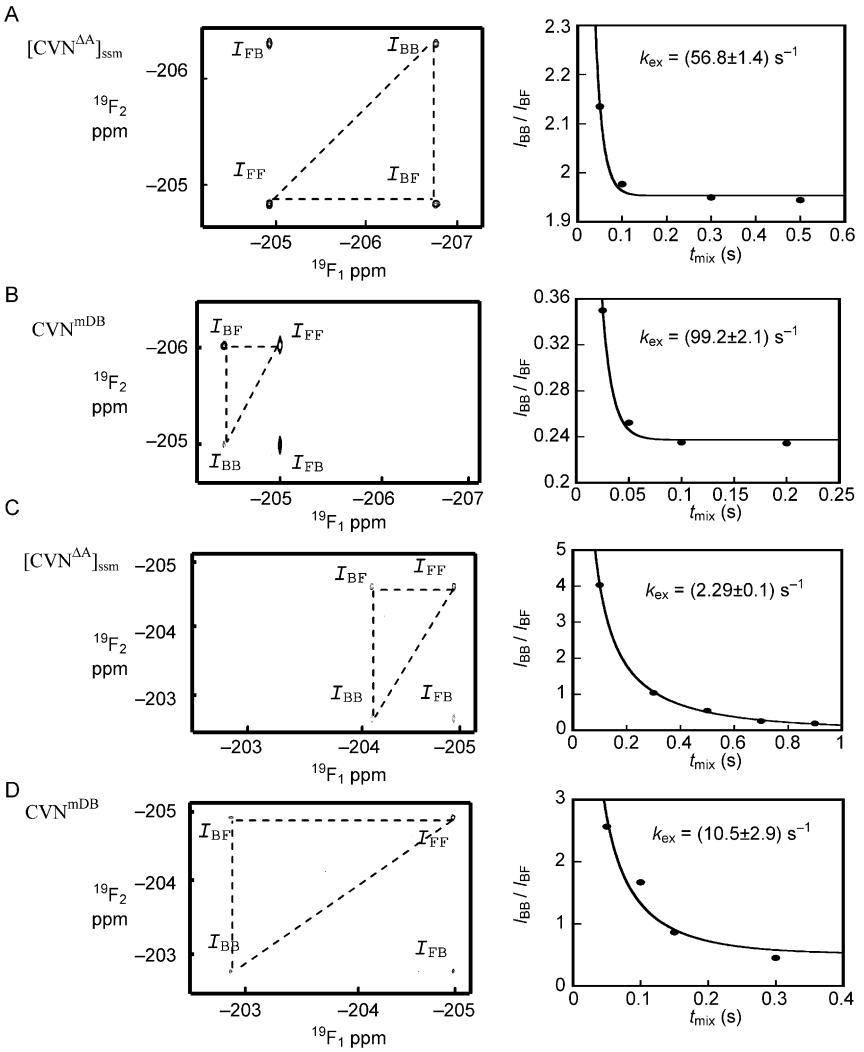

Figure 3. 2D ^{19}F-^{19}F NOESY exchange spectra of ^{19}F-Man2/Man3 in the presence of $[CVN^{\Delta A}]_{ssm}$ and CVN^{mDB} protein; A) ^{19}F-Man2 (200 μM) bound to $[CVN^{\Delta A}]_{ssm}$(left panel; $t_{mix} = 0.1$ s), and the exchange curve of bound/bound over free/bound intensity ratio (I_{BB}/I_{BF}) versus mixing time (right panel) t_{mix}: 0.05, 0.1, 0.3, 0.5 s; B) ^{19}F-Man2 bound to CVN^{mDB} (left panel; $t_{mix} = 0.05$ s) and the exchange curve of bound/bound over free/bound intensity ratio (I_{BB}/I_{BF}) versus mixing time (right panel) t_{mix}: 0.025, 0.05, 0.1, 0.2 s; C) ^{19}F-Man3 (50 μM) bound to $[CVN^{\Delta A}]_{ssm}$ (left panel; $t_{mix} = 0.1$ s) and the exchange curve of bound/bound over free/bound intensity ratio (I_{BB}/I_{BF}) versus mixing time (right panel) t_{mix}: 0.1, 0.3, 0.5, 0.7, 0.9 s; D) ^{19}F-Man3 (50 μM) bound to CVN^{mDB} (left panel; $t_{mix} = 0.05$ s) and the exchange curve of bound/bound over free/bound intensity ratio (I_{BB}/I_{BF}) versus mixing time (right panel) t_{mix}: 0.05, 0.1, 0.15, 0.3 s. All spectra were recorded at 280 K for 1:1 molar ratios. The auto-correlation (diagonal) peaks I_{FF} and I_{BB} arise from the free and bound states, whereas cross-correlation (off-diagonal) peaks $I_{FB} = I_{BF}$ report on the exchange between the free and bound states.

cross-peak (I_{BB}/I_{BF}) as a function of mixing time are shown next to the NOESY spectra. Analysis of the exchange curve for ^{19}F-Man2 when bound to the site on domain B yields a free to bound exchange rate (k_{ex}) of $56.8\pm1.4\ s^{-1}$, whereas that for binding to domain A yields a k_{ex} value of $99.2\pm2.1\ s^{-1}$.

The equivalent data of ^{19}F-Man3 (50 μM) in the presence of $[CVN^{\Delta A}]_{ssm}$ and CVN^{mDB} (1:1 molar ratio) are shown in Figures 3C and 3D and resulted in k_{ex} values of $2.29\pm0.1\ s^{-1}$ and $10.5\pm2.9\ s^{-1}$ for the binding to domains B and A, respectively. Thus, the exchange between the free and bound states of the di- and trimannoside is somewhat faster from domain A than domain B. Although easily observed at 280 K, no exchange peak was observed at 298 K for ^{19}F-Man2 due to intermediate exchange that caused line broadening beyond detection. The peaks for ^{19}F-Man3, on the other hand, are still present at 298 K.

Protein-detected binding between ^{19}F-Man2 and ^{19}F-Man3 with CV-N: Direct protein-observed NMR titration experiments were carried out with ^{19}F-Man2 at 298 K by following chemical shift perturbations in the ^{1}H-^{15}N HSQC spectrum of ^{15}N uniformly labeled $[CVN^{\Delta A}]_{ssm}$ (75 μM, Figure 4) and CVN^{mDB} (400 μM, the Supporting Information, Figure S1) as a function of added sugar. Spectra in the absence (black contours) and presence (green contours) of 25 molar equivalents of ^{19}F-Man2 are provided in Figure 4A and the Supporting Information (Figure S1A), respectively. In the ^{1}H-^{15}N HSQC NMR spectra of $[CVN^{\Delta A}]_{ssm}$ and CVN^{mDB} titrations at 298 K, resonances are in fast exchange, which is in contrast to the situation in the ^{19}F NMR spectra in which resonances at 298 K were in intermediate exchange and broadened beyond detection. Following the chemical shift changes throughout the titration yielded the binding isotherm displayed in the right panels of Figure 4A and the Supporting Information (Figure S1A), respectively.

The equilibrium dissociation constant (K_D^F) for ^{19}F-Man2 binding was determined from the titration shifts (chemical shift $\Delta\delta$ (ppm) vs. the ratio of ligand to protein concentration) by using several resonances. ^{19}F-Man2 binding to the single sites on domains B and A yielded K_D^F values of 960 ± 91 μM and 1.37 ± 0.075 mM, respectively. The latter value is about a factor of two larger than the one determined for Man2 binding to site A on CVN^{mutDB} (757 ± 80 μM),[36] suggesting that the substitution of fluorine at the 2′ position reduces the binding affinity only by a very small amount. As noted previously, Man2 exhibits a slight preference for Domain B over Domain A, respectively.[28,31,32]

Equivalent NMR titration experiments, monitoring the chemical shift perturbations in the ^{1}H-^{15}N HSQC spectra of $[CVN^{\Delta A}]_{ssm}$ and CVN^{mDB} were carried out at 280 K with ^{19}F-Man3. A superposition of $[CVN^{\Delta A}]_{ssm}$ (50 μM) spectra in the absence (black contours) and presence (green contours) of 3 molar equivalents of ^{19}F-Man3 is provided in Figure 4B. The binding isotherm derived from the intensity changes of free resonances is depicted in the right panel. The equivalent titration experiment was performed for CVN^{mDB} (50 μM) and the data are provided in the Supporting Information (Figure S1B). The dissociation constants were extracted as described for ^{19}F-Man2 (above) and binding to a single site on domain B (in $[CVN^{\Delta A}]_{ssm}$) yielded a K_D^F value of 63.5 ± 5 μM, whereas the one for binding to a single site on domain A (in CVN^{mDB}) was 150.3 ± 7 μM.

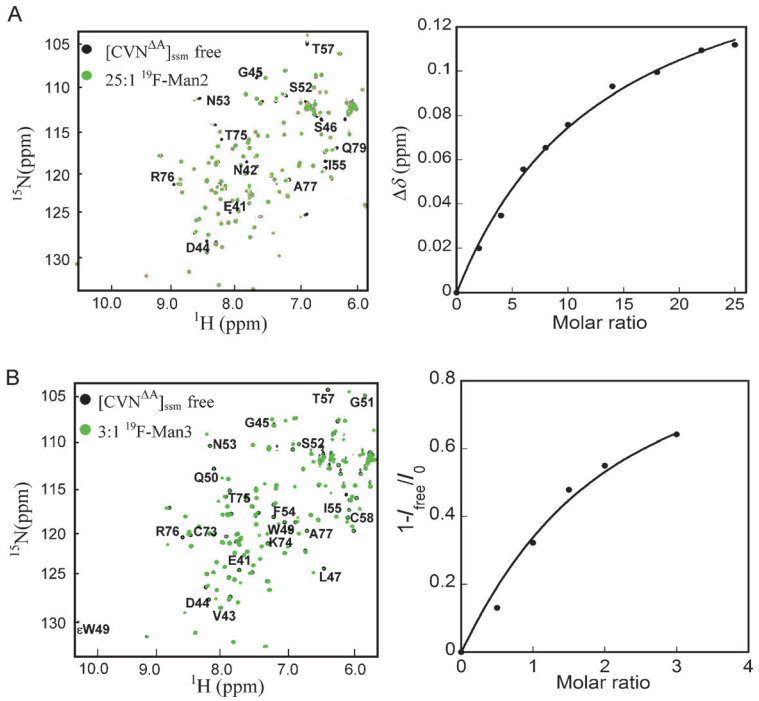

Figure 4. NMR titration of $[CVN^{\Delta A}]_{ssm}$ with ^{19}F-Man2 recorded at 298 K and ^{19}F-Man3 recorded at 280 K, respectively. A) Perturbed amide resonances in the $[CVN^{\Delta A}]_{ssm}$ spectrum clearly reside in domain B and are labeled by amino acid name and number. The left panel display a superposition of ^{1}H-^{15}N HSQC NMR spectra of $[CVN^{\Delta A}]_{ssm}$ in the absence (black) and presence of 25 molar equivalents of ^{19}F-Man2 (green). The right panel displays the titration curve (chemical shift difference vs. ligand/protein molar ratio), with the chemical shift difference defined as: $\Delta\delta=[(\Delta\delta_H)^2+(\Delta\delta_N\times0.17)^2]^{1/2}$, in which $\Delta\delta_H$ and $\Delta\delta_N$ are the observed chemical shift changes for ^{1}H and ^{15}N, respectively. The system is in fast exchange, as evidenced by a single signal corresponding to glycan-free and glycan-bound $[CVN^{\Delta A}]_{ssm}$; B) Superposition of ^{1}H-^{15}N HSQC spectra of $[CVN^{\Delta A}]_{ssm}$ (50 μM) in the absence (black) and presence (green) of 3 molar equivalents of ^{19}F-Man3 (left panel). The right panel displays the titration curve at glycan/protein molar ratios: 0:1, 0.5:1, 1:1, 1.5:1, 2:1, and 3:1. The system is in slow exchange, as evidenced by separate signals for glycan free and glycan bound $[CVN^{\Delta A}]_{ssm}$. The binding isotherm is derived from the relative signal intensities ($1-I_{free}/I_0$) (right panel).

ITC binding: A direct comparison of binding parameters that were extracted from the different NMR titrations with those from ITC measurements was performed.

In particular, reverse titrations in which ^{19}F-Man3 (50 μM) was placed into the cell and protein into the injector were carried out. In this manner, an equivalent situation to the one in ^{19}F-glycan-observed NMR titrations at 280 K is created. The measured titration heat as well as the derived binding isotherms are provided in Figure 5A and the Supporting Information (Figure S2A) for $[CVN^{\Delta A}]_{ssm}$ and CVN^{mDB}, respectively. The extracted K_D^F values were 12.6±1.2 μM for $[CVN^{\Delta A}]_{ssm}$ and 28.5±3.5 μM for CVN^{mutDB}, which are in excellent agreement with the values extracted from the ^{19}F-glycan-observed NMR titrations (see above).

We also carried out direct ITC titrations at 280 K with ^{19}F-Man3 in the injector and $[CVN^{\Delta A}]_{ssm}$(30 μM) and CVN^{mDB}(50 μM) in the cell. The observed binding isotherms are provided in Figure 5B and the Supporting Information (Figure S2B), yielding K_D^F values of 62.5±2 μM and 153.3±5 μM for $[CVN^{\Delta A}]_{ssm}$ and CVN^{mDB}, respectively. These values are in good agreement with those obtained from the NMR direct titration experiment for both $[CVN^{\Delta A}]_{ssm}$ and CVN^{mDB} variants, which were 63.5±5 μM and 150.3±7 μM, respectively. Interestingly, it appears that ^{19}F-Man3 no longer preferentially binds to domain A, as was observed for the non-fluorinated Man3,[28,31,32] possibly due to the ^{19}F substitution. The extracted dissociation constants for ^{19}F-Man3 binding are provided in Table 1.

Table 1. Dissociation constants for the interaction of ^{19}F-Man3 with single binding site CV-N variants determined by ligand-observed ^{19}F NMR spectroscopy, reverse ITC, protein-observed NMR, and direct ITC experiments.

Protein	K_D^F [μM] ^{19}F NMR	K_D^F [μM] reverse ITC	K_D^F [μM] ^{1}H-^{15}N HSQC	K_D^F [μM] direct ITC
$[CVN^{\Delta A}]_{ssm}$	10.8±0.3	12.6±1.2	63.5±5	62.5±2
CVN^{mDB}	33.5±3.5	28.5±3.5	150.3±7	153.3±5

Calorimetry is the only technique that directly permits to evaluate the basic physical forces in sufficient detail between and within molecules by measuring heat quantities or heat effects.[42] Therefore, a deeper understanding of the molecular basis of protein–ligand interactions can be gained by thoroughly characterizing and quantifying the energetics that govern complex formation.[24,42] Analysis of the reverse ITC binding isotherm for the ^{19}F-Man3 titrations with $[CVN^{\Delta A}]_{ssm}$ yielded a ΔG value of −5.1 kcal mol^{-1}, ΔH = −2.9 kcal mol^{-1}, and a binding entropy ($T\Delta S$) of 2.2 kcal mol^{-1}, whereas for the direct ITC titration, a ΔG value of −5.3 kcal mol^{-1}, ΔH = −5.1 kcal mol^{-1}, and $T\Delta S$ of 0.2 kcal mol^{-1} was obtained. Similarly, a ΔG value of −5.8 kcal mol^{-1}, ΔH = −1.5 kcal mol^{-1}, and $T\Delta S$ of 4.3 kcal mol^{-1} was measured in the reverse ITC titration of ^{19}F-Man3 with CVN^{mDB}, whereas a ΔG value of −4.88 kcal mol^{-1}, ΔH = −4.08 kcal mol^{-1}, and $T\Delta S$ of 0.8 kcal mol^{-1} was obtained for the direct titration. A summary of all thermodynamic data determined for ^{19}F-Man3 binding to $[CVN^{\Delta A}]_{ssm}$ and CVN^{mDB} in reverse and direct ITC titrations is provided in Table 2.

For both mutants, binding to ^{19}F-Man3 was driven by enthalpic contributions (with negative ΔH values of −2.9 kcal mol^{-1} and −5.1 kcal mol^{-1} in the case of $[CVN^{\Delta A}]_{ssm}$, and −1.5 kcal mol^{-1} and −4.08 kcal mol^{-1} for CVN^{mDB}, for the reverse and direct ITC titrations, respectively), with favorable entropic contributions. Somewhat larger positive $T\Delta S$ values (2.2 kcal mol^{-1} for $[CVN^{\Delta A}]_{ssm}$ and 4.3 kcal mol^{-1} for CVN^{mDB})

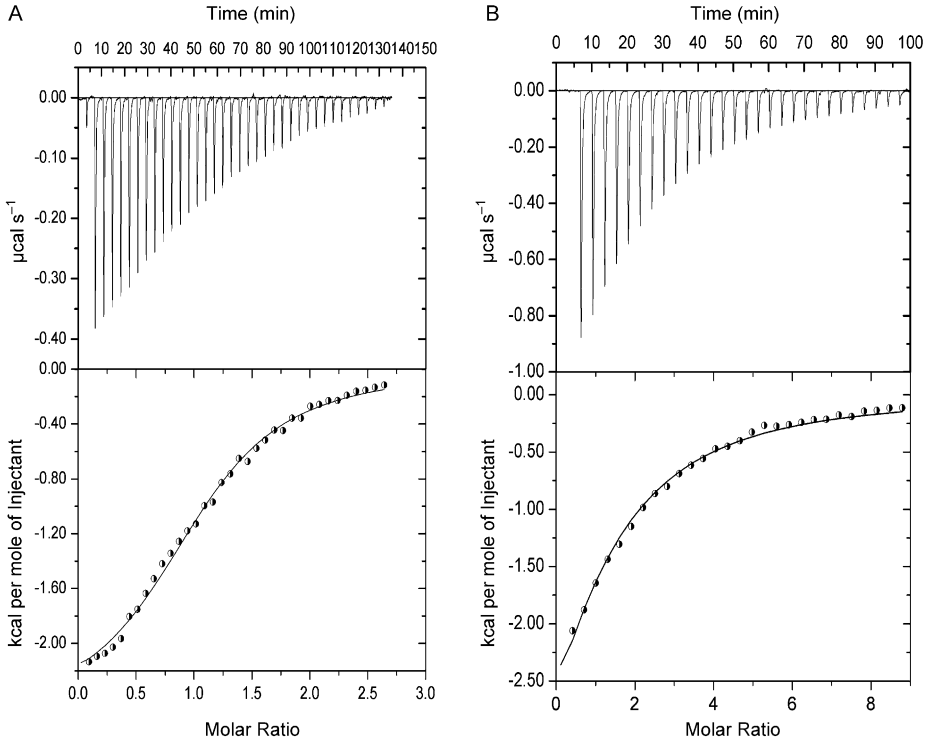

Figure 5. ITC titration experiments for the interaction between ^{19}F-Man3 and $[CVN^{\Delta A}]_{ssm}$ at 280 K. A) The trace for titrating $[CVN^{\Delta A}]_{ssm}$ into ^{19}F-Man3 (50 μM; reverse titration) for 28 automated injections is shown (top panel), and the derived binding isotherm is displayed in the bottom panel. The nonlinear least-squares best fit to the experimental data using a one-site model is shown by the solid line; B) The ITC trace of titrating ^{19}F-Man3 into $[CVN^{\Delta A}]_{ssm}$ (30 μM; direct titrations) for 28 automated injections (top panel) with the derived binding isotherm (bottom panel) is displayed. The nonlinear least-squares best fit to the experimental data by using a one-site model is shown by the solid line.

Table 2. Thermodynamic parameters extracted from the ITC binding data.

Protein	Enthalpy (ΔH) [kcal mol^{-1}]	Entropy ($T\Delta S$) [kcal mol^{-1}]	Free energy (ΔG) [kcal mol^{-1}]	Stoichiometry (n)
$[CVN^{\Delta A}]_{ssm}$ reverse ITC	-2.9 ± 0.05	2.2 ± 0.04	-5.1 ± 0.06	1.01 ± 0.03
$[CVN^{\Delta A}]_{ssm}$ direct ITC	-5.1 ± 0.1	0.2 ± 0.08	-5.3 ± 0.1	1.0 ± 0.0
CVN^{mDB} reverse ITC	-1.5 ± 0.03	4.3 ± 0.02	-5.8 ± 0.04	1.02 ± 0.04
CVN^{mDB} direct ITC	-4.08 ± 0.06	0.8 ± 0.03	-4.88 ± 0.05	1.0 ± 0.0

The errors listed are standard deviations of the fits.

were obtained for the reverse ITC titrations, compared with the direct ones (0.2 kcal mol^{-1} for $[CVN^{\Delta A}]_{ssm}$ and 0.8 kcal mol^{-1} for CVN^{mDB}), suggesting that water molecules are more efficiently released from the complex surface in the case of reverse titrations.[42] The overall ΔG values, however, are not very different.

ITC also allows the stoichiometry of binding to be determined, independent of the binding affinity.[24] Since a 1:1 stoichiometry was obtained from the experimental (sigmoid) curves in the cases of reciprocal ITC titrations, a one binding site model was used to fit the data, from which the binding-affinity parameters were extracted. In the case of direct ITC titrations, since $\approx$1:1 stoichiometry was observed, a stoichiometry value of $n=1$ was fixed to fit the experimental (parabolic) curves, consistent with the detection of a single binding site for the equivalent, protein-observed ^{1}H-^{15}N HSQC titrations (Figure 4B and the Supporting Information, Figure S1B). Furthermore, the fully saturated samples that resulted either at the end of protein-observed ^{1}H-^{15}N HSQC or direct ITC titrations, were tested by using 1D-^{19}F NMR, and indeed, only a single protein-bound peak, corresponding to one binding site, was observed. Therefore, the reverse titration allowed us not only to check the stoichiometry, but also to ensure that a suitable binding model was used to fit the ITC data. For a 1:1 binding stoichiometry, the measured thermodynamic parameters are expected to be invariant when changing the orientation of the experiment.[24] However, this is rarely the case since one of the two species may display greater aggregation or less solubility when concentrated.[24b] Indeed, a comparison of the data in Table 1 revealed that titrating ^{19}F-Man3 into solutions of $[CVN^{\Delta A}]_{ssm}$ and CVN^{mDB} by using protein-observed ^{1}H-^{15}N HSQC spectra or direct ITC experiments yielded approximately five times higher K_D^F values than those obtained from ligand-observed ^{19}F NMR and reciprocal ITC titrations. Naturally, if aggregation occurs, this will happen at high concentrations of the ligand. Therefore, it is advantageous to measure the binding on the ligand, either by NMR spectroscopy or reverse ITC, since lower ligand concentrations are needed.

Thus, ligand-detected binding methods are preferable compared with methods that measure protein signals, because any errors associated with solubility that may result in incorrect ligand concentrations are avoided.

Detection of a second binding mode in the interaction of ^{19}F-Man3 with CV-N: The concentration of ^{19}F-Man3 in the ligand-detected ^{19}F NMR experiments was 50 μM, whereas for those with ^{19}F-Man2 it was 200 μM. To directly compare the results of $[CVN^{\Delta A}]_{ssm}$, CVN^{mDB} and $CV\text{-}N^{P51G}$ binding to the two fluorinated glycans, we also recorded a ligand-detected ^{19}F-spectrum of ^{19}F-Man3 (200 μM) with CV-N variants (1:1 molar ratio). As can be observed from the comparison of the spectra illustrated in Figure 6, at higher ^{19}F-Man3 concentrations (>150 μM), additional resonances emerge. These new resonances exhibit exactly the same chemical shifts (Figure 6B) that were seen for the signals of ^{19}F-Man2 when bound to domains A and B of CV-N, respectively (Figure 6A).

The presence of the second binding mode can also be observed in the 2D ^{19}F-^{19}F exchange NOESY experiment recorded with a 50 ms mixing time on the sample of ^{19}F-Man3 (200 μM) with $[CVN^{\Delta A}]_{ssm}$ and CVN^{mDB} (Figure 6C). Given that the additional peaks exactly match the chemical shifts of the bound conformations of ^{19}F-Man2 when sitting in domains A and B of CV-N, and are only observed at relatively high concentrations, it appears that each domain of CV-N binds first to the Manα(1-2)Manα unit that is closer to O-methyl group in ^{19}F-Man3 (high affinity binding mode: 1) and subsequently to the non-reducing end ^{19}F-Manα(1-2)Manα unit (low affinity binding mode: 1′).

To further substantiate our findings we also carried out a competition binding experiment, by adding non-fluorinated Man2 to a solution of ^{19}F-Man3 (200 μM) and $[CVN^{\Delta A}]_{ssm}$ (1:1 molar ratio) and monitored the change in 1D-^{19}F NMR ligand signal intensity as a function of Man2 addition. The resulting data up to a 20 fold molar excess of Man2, are provided in Figure 6D.

As can be noted, the resonance that corresponds to the bound conformation of the non-reducing end ^{19}F-Manα(1-2)Manα unit is the one that is affected first by the addition of non-fluorinated Man2, whereas the resonance corresponding to the bound conformation of the second Manα(1-2)Manα unit (the one closer to O-methyl group) is affected only at a higher Man2 addition. Such differentiation was not observed when ^{19}F-Man3 or non-fluorinated Man3 was used in protein-detected titration experiments.

^{19}F NMR competition assay: To further highlight the advantages of using ^{19}F NMR spectroscopy, we also carried out a quantitative competition binding experiment, titrating non-fluorinated Man3 into a complex of ^{19}F-Man3 (250 μM) with relatively low concentration (25 μM) of CVN^{mDB} (10:1 molar ratio), which ensures that only the high affinity binding mode is involved. Indeed, inspection of the 1D-^{19}F NMR spectra reveals only the presence of the peak corresponding to the high affinity protein–ligand binding mode, whereas no additional low affinity binding peak is observed.

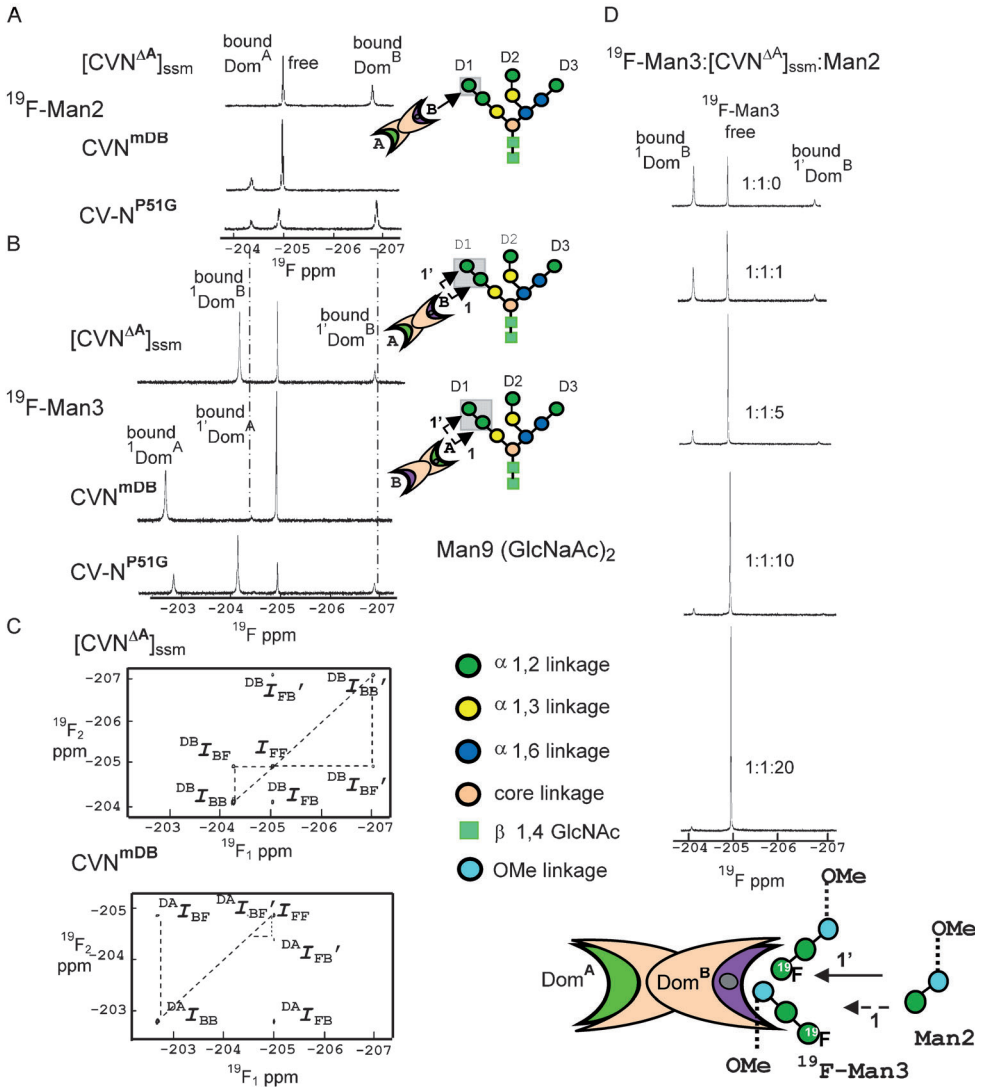

Figure 6. 1D-^{19}F NMR spectra of ^{19}F-Man2/Man3 (200 μM) in the presence of different CV-N variants, which illustrates the power of ^{19}F NMR spectroscopy for discriminating between different binding sites and modes. The presence of a second binding mode for the interaction of CV-N with ^{19}F-Man3 is clearly observed. All spectra were recorded at 280 K. A) 1D-^{19}F spectra of ^{19}F-Man2 (200 μM) in the presence of $[CVN^{\Delta A}]_{ssm}$, CVN^{mDB} and $CV\text{-}N^{P51G}$. B) 1D-^{19}F spectra of ^{19}F-Man3 (200 μM) in the presence of $[CVN^{\Delta A}]_{ssm}$, CVN^{mDB} and $CV\text{-}N^{P51G}$. Schematic depiction of ^{19}F-Man2 and the two modes of ^{19}F-Man3 binding to CV-N in the right-side panels of A) and B). The individual sugar units on the oligosaccharide are color coded according to their linkage pattern; C) 2D ^{19}F-^{19}F NOESY spectra of ^{19}F-Man3 in the presence of $[CVN^{\Delta A}]_{ssm}$ and CVN^{mDB} (200 μM; 1:1 molar ratio of glycan/protein). The auto-correlation (diagonal) peak intensities I_{FF} and I_{BB} in the 2D ^{19}F-^{19}F NOESY spectra arise from the free and bound states, whereas the cross-correlation (off-diagonal) resonances $I_{FB}=I_{BF}$ and $I_{FB'}=I_{BF'}$ arise from exchange between the two binding modes for CV-N and ^{19}F-Man3; D) Competitive binding of Man2 to the complex of ^{19}F-Man3/$[CVN^{\Delta A}]_{ssm}$ (200 μM;^{19}F-Man3/$[CVN^{\Delta A}]_{ssm}$/Man2 molar ratios were: 1:1:0; 1:1:1; 1:1:5; 1:1:10; and 1:1:20). A schematic representation of Man2 competing with ^{19}F-Man3 binding to $[CVN^{\Delta A}]_{ssm}$ is shown in the bottom panel. The Man2 competitor first displaces the ^{19}F-Man3 bound to protein with the non-reducing ^{19}F-Manα(1-2)Manα unit (the low affinity binding mode shown as a solid arrow), and later the one bound with the unit closer to the O-methyl group (high affinity binding mode shown as a dashed arrow).

The intensity change in the 1D-^{19}F NMR free ligand signal was monitored as a function of Man3 addition. A schematic representation of the competitive binding scenario is illustrated in Figure 7A, and the resulting data are provided in Figure 7B. The intensity increase in the 1D-^{19}F NMR spectrum of the free ^{19}F-Man3 signal in complex with CVN^{mDB}, upon addition of the non-fluorinated competitor (Man3), corresponds to the amount of non-labeled ligand bound to CVN^{mDB}. The dissociation constant of Man3 binding to CVN^{mDB} was obtained from the relevant competition titration data for the ^{19}F-Man3/CVN^{mDB}/Man3 complex (Figure 7B). To extract the binding constant k_d of Man3 interacting with CVN^{mDB}, it is necessary to know the K_D^F value of ^{19}F-Man3 binding to CVN^{mDB} (Figure 7A). We determined this value by ^{19}F NMR spectroscopy and reciprocal ITC titrations (see above). The extracted k_d value of 4.65 ± 0.6 μM is consistent with our previous affinity data of

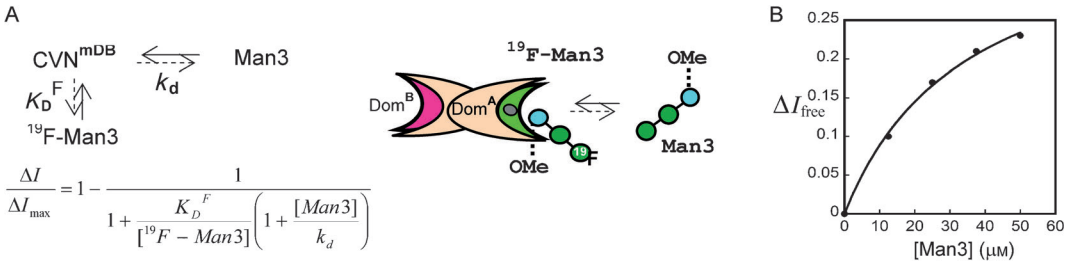

$$\frac{\Delta I}{\Delta I_{max}} = 1 - \frac{1}{1 + \frac{K_D^F}{[^{19}F - Man3]}\left(1 + \frac{[Man3]}{k_d}\right)}$$

Figure 7. Competition of Man3 and ^{19}F-Man3 for ^{19}F-Man3 (250 μM) in complex with CVN^{mDB} (25 μM). A) Schematic representation of the competitive binding scenario. Cheng–Prusoff equation based on a competitive site binding model, in which [^{19}F-Man3] and [Man3] are the concentrations of the fluorinated and non-fluorinated ligand, and K_D^F the dissociation constants of ^{19}F-Man3 interacting with the glycan-binding site on domain A of CVN^{mDB}. The data were fitted using the maximum increase in the free ^{19}F-Man3 resonance intensity upon Man3 addition, with ΔI_{max}, and k_d the dissociation constant for Man3 binding as adjustable parameters; B) Titration curve extracted from ^{19}F NMR spectra that were recorded for ^{19}F-Man3/CVN^{mDB}/Man3 molar ratios of 10:1:0, 10:1:0.25, 10:1:0.5, 10:1:0.75, and 10:1:1. In the titration curve, the bound fraction of Man3 is given by the difference in signal intensity of the ^{19}F-Man3 free signal $\Delta I = I_{free} - I_0$ during the titration, in which I_{free} is the intensity of the ^{19}F-Man3 free signal at each point in the titration, and I_0 the intensity of the ^{19}F-Man3 free signal at the beginning of the titration.

the non-labeled Man3 with CVN^{mDB} (3.4 ± 0.05 μM), obtained from an ITC titration experiment.[36]

Conclusion

We have presented an approach to quantitatively assess glycan–lectin interactions by monitoring the changes in the ^{19}F NMR resonances of fluorinated glycans upon protein addition. Our method exploits the relatively large ^{19}F NMR chemical shift range that results in well resolved resonances in the 1D spectrum. Employing fluorinated ligands permits the analysis protein–ligand interactions by ^{19}F NMR spectroscopy, even for high molecular mass proteins (>100 kDa) and requires only minimal amounts of ligand. Therefore, new avenues for screening in a facile fashion and relatively short time can be envisaged.

In particular we show that:

1) Quantitative binding affinity data can be obtained using ^{19}F NMR experiments with fluorinated glycans.
2) Information about protein–ligand binding exchange can be extracted from ^{19}F-^{19}F NOESY experiments and we determined the chemical exchange rate constant, k_{ex}, for each of the two binding sites of CV-N.
3) Different binding modes can be discerned for the two neighboring Manα(1-2)Manα units in ^{19}F-Man3 when interacting with CV-N.
4) ^{19}F NMR competition experiments can be employed for quantitatively extracting affinity constants of non-fluorinated glycans with target lectins.

In summary, utilizing ^{19}F as a sensor for studying protein–ligand interactions represents a promising perspective for ^{19}F NMR spectroscopy, as a universal tool in drug discovery for any target receptors for which fluorinated ligands are available or can be synthesized.

Experimental Section

Lectins: The Cyanovirin-N wild-type stabilized variant CV-N^{P51G} and the two mutants [CVN$^{\Delta A}$]$_{ssm}$ and CVN^{mDB} that possess only one sugar-binding site, either in domain B ([CVN$^{\Delta A}$]$_{ssm}$) or domain A (CVN^{mDB}) were prepared as described previously.[35–37] The two fluoro-deoxy sugar derivatives, methyl 2-deoxy-2-fluoro-α-D-mannopyranosyl-(1→2)-α-D-mannopyranoside and methyl 2-deoxy-2-fluoro-α-D-mannopyranosyl-(1→2)-α-D-mannopyranosyl-(1→2)-α-D-mannopyranoside were obtained using synthetic procedures outlined in the Supporting Information (Scheme S1).

Cell assays: CV-N^{P51G} was fluorescently labeled by fluorescein isothiocyanate under activity-preserving conditions, separated from reagents by gel filtration, and applied in cytofluorometry as described for other lectins previously.[43]

NMR spectroscopy: ^{19}F NMR spectra were recorded on a Bruker 600 MHz AVANCE spectrometer, equipped with a Bruker CP TXO triple-resonance, X-nuclei observe, *z*-axis gradient cryoprobe (Bruker Biospin, Billerica, MA). ^{1}H-^{15}N HSQC experiments were recorded on a Bruker 600 MHz AVANCE spectrometer equipped with CP TCI triple-resonance, *z*-axis gradient ^{1}H detect cryoprobe (Bruker Biospin, Billerica, MA). Spectra were processed with NMRPipe[44] and analyzed with NMRview.[45]

NMR titrations: *Monitoring the resonances of the fluorinated ligand*: Ligand-observed ^{19}F NMR experiments were performed using fluorinated deoxy-sugars, ^{19}F-Man2 (200 μM) and ^{19}F-Man3 (50 μM), and the single binding site variants, [CVN$^{\Delta A}$]$_{ssm}$ and CVN^{mDB}, as well as the stabilized CV-N^{P51G} wild-type protein at 1:1 protein/ligand molar ratios, in sodium phosphate buffer (20 mM), pH 6.0, 0.01% NaN_3, 90% H_2O/10% D_2O.

For titration experiments with ^{19}F-Man3 sugars (50 μM), ^{19}F-spectra were monitored upon addition of increasing amounts of protein, [CVN$^{\Delta A}$]$_{ssm}$ and CVN^{mDB}, (5 mM stock solution) in sodium phosphate buffer (20 mM), pH 6.0, 0.01% NaN_3, 90% H_2O/10% D_2O. A series of 1D-^{19}F NMR spectra were recorded at 280 K at protein/sugar molar ratios of 0:1, 0.5:1, 1:1, and 1.5:1 for [CVN$^{\Delta A}$]$_{ssm}$ and 0:1, 0.5:1, 1:1, 2:1 and 3:1 for CVN^{mDB}. Free and bound ^{19}F ligand resonances throughout the titration are in slow exchange on the chemical shift scale. The observed signal intensity change during the titrations is directly proportional to the fraction bound (f_b) and is given by: $f_b = 1 - f_f = 1 - I_{free}/I_0 = [PL]/[L]$, in which [L] is the total concentration of ligand and [PL] the concentration of the resulting ligand-protein complex; I_{free} is the NMR peak intensity of the free ligand signal at each point in the titration, and I_0 is the peak intensity of the free ligand signal at the beginning of the titration. Binding curves were derived from the relative ratios of ligand resonance intensities ($1 - I_{free}/I_0$) versus the molar ratio (M) of protein/sugar, and apparent K_D^F values were obtained by non-linear best fitting of the titration curves using KaleidaGraph (Synergy Software, Reading, PA), by using Equation (1).

$$f_b = 1 - \frac{I_{\text{free}}}{I_0} = 0.5^* \left(M + 1 + \frac{K_D^F}{[L]} - \sqrt{\left(M + 1 + \frac{K_D^F}{[L]} \right)^2 - 4M} \right) \quad (1)$$

Monitoring the protein resonances: The protein-observed NMR titration experiments were performed on Bruker 600 MHz AVANCE spectrometers, equipped with 5 mm, triple resonance, three-axis gradient probes or *z*-axis gradient cryoprobes, by using uniformly ^{15}N-labeled $[CVN^{\Delta A}]_{ssm}$-(75 μM) or CVN^{mDB}(400 μM) with increasing amounts of ^{19}F-Man2, in sodium phosphate buffer (20 mM), pH 6.0, 0.01 % NaN_3, 90 % H_2O/10 % D_2O. A series of ^{1}H-^{15}N HSQC spectra at 298 K were recorded after the addition of sugar aliquots from a stock solution (10 mM) at sugar/protein molar ratios of: 1:0, 2:1, 4:1, 6:1, 8:1, 10:1, 14:1, 18:1, 22:1, and 25:1 for $[CVN^{\Delta A}]_{ssm}$ and 0:1, 0.5:1, 1:1, 1.5:1, 2:1, 2.5:1, 3:1, 3.5:1, 5:1, 6:1, 7:1, 8:1, 9:1, 11:1, 12:1, 15:1, 16:1, 21:1, and 25:1 for CVN^{mDB}.

Free and sugar-bound protein resonances throughout the titration are in fast exchange on the chemical shift scale. The observed chemical shift change during the titration is given by: $\Delta\delta = [PL]/[P]\ (\delta_b - \delta_f)$, in which [P] and [PL] are the concentrations of protein and ligand–protein complex and δ_b and δ_f are the chemical shifts of protein resonances in the free and fully bound state. The chemical shift difference was calculated as: $\Delta\delta = [(\Delta\delta_H)^2 + (\Delta\delta_N \times 0.17)^2]^{1/2}$, in which $\Delta\delta_H$ and $\Delta\delta_N$ represent the observed chemical shift changes for ^{1}H and ^{15}N, respectively. The dissociation constant K_D^F, was obtained by best fitting the titration curve (chemical shift change $\Delta\delta$ vs. molar ratio M of sugar/protein) using KaleidaGraph software and Equation (2):

$$\Delta\delta = 0.5^* \Delta\delta_{\max} \left(M + 1 + \frac{K_D^F}{[P]} - \sqrt{\left(M + 1 + \frac{K_D^F}{[P]} \right)^2 - 4M} \right) \quad (2)$$

Analogous NMR titration experiments were performed by using uniformly ^{15}N-labeled $[CVN^{\Delta A}]_{ssm}$(50 μM) and CVN^{mDB}(50 μM) with ^{19}F-Man3, in sodium phosphate buffer (20 mM), pH 6.0, 0.01 % NaN_3, 90 % H_2O/10 % D_2O. A series of ^{1}H-^{15}N HSQC spectra were recorded at 280 K after addition of sugar aliquots from a stock solution of 10 mM at sugar/protein molar ratios of: 0:1, 0.5:1, 1:1, 1.5:1, 2:1, and 3:1 for $[CVN^{\Delta A}]_{ssm}$ and 0:1, 0.5:1, 1:1, 1.5:1, 2:1, 2.5:1, 3.5:1, and 4:1 for CVN^{mDB}. In this case, free and sugar-bound protein resonances throughout the titration were in slow exchange on the chemical shift scale. The observed signal intensity change during the titration is direct proportional to the fraction bound (f_b), given by: $f_b = 1 - f_f = 1 - I_{free}/I_0 = [PL]/[P]$, in which [P] is the total concentration of protein and [PL] the concentrations of the protein–ligand complex. I_{free} is the resonance intensity of the ligand-free protein signal at each point in the titration, and I_0 is the resonance intensity of the ligand-free protein signal at the beginning of titration. Binding curves were derived from the relative ratios of ligand resonance intensities ($1 - I_{free}/I_0$) versus the molar ratio (M) of protein/sugar, and apparent K_D^F values were obtained by non-linear best fitting of the titration curves using KaleidaGraph (Synergy Software, Reading, PA), averaging over the eight titration curves by using Equation (3):

$$f_b = 1 - \frac{I_{free}}{I_0} = 0.5 \times \left(M + 1 + \frac{K_D^F}{[P]} - \sqrt{\left(M + 1 + \frac{K_D^F}{[P]} \right)^2 - 4M} \right) \quad (3)$$

2D ^{19}F-^{19}F NOESY exchange experiment: Two-dimensional exchange spectroscopy (NOESY) represents a powerful tool for probing the ligand–receptor exchange.[46] NOESY experiments are particularly suitable to evaluate chemical exchange processes that occur on a slow time scale, in which the exchange rate has little effect on the line shape. A series of 2D homonuclear exchange ^{19}F-^{19}F NOESY experiments were recorded at 280 K on a sample containing 200 μM ^{19}F-Man2, complexed with $[CVN^{\Delta A}]_{ssm}$ and CVN^{mDB} at 1:1 molar ratios and mixing times (t_{mix}) of 0.05, 0.1, 0.3, 0.5 s, and 0.025 0.05, 0.1, 0.2 s, respectively. An equivalent series was recorded for 50 μM ^{19}F-Man3, complexed with $[CVN^{\Delta A}]_{ssm}$ and CVN^{mDB} at mixing times (t_{mix}) of 0.1, 0.3, 0.5, 0.7, 0.9 s and 0.05, 0.1, 0.15, 0.3 s, respectively. The exchange rate constant was extracted by fitting the experimental intensity ratios (diagonal peak (I_{BB}) of bound conformation, to that of the bound to free exchange cross-peak (I_{BF})) versus mixing time (t_{mix}), by using Equation (4), in which k_{eq} is the equilibrium constant and k_{ex} is the free–bound exchange rate.[47]

$$\frac{I_{BB}}{I_{BF}} = \frac{k_{eq}[\exp(k_{ex} \times t_{mix}) + 1]}{[\exp(k_{ex} \times t_{mix}) - 1]} \quad (4)$$

Isothermal titration calorimetry: Calorimetric titrations were performed using a VP-ITC isothermal titration calorimeter (MicroCal, LLC; Northampton, MA). Titrations were carried out at 280 K and all solutions contained sodium phosphate buffer (50 mM), pH 7.4, 0.2 M NaCl, 0.02 % NaN_3. ITC measurements were carried out with $[CVN^{\Delta A}]_{ssm}$ and CVN^{mDB} solution in the cell (ca. 1.44 mL active volume) at 30 μM and 50 μM concentrations, respectively, and stirred at 310 rpm. 28 injections of 10 μL aliquots of ^{19}F-Man3 (2.5 mM) in the case of $[CVN^{\Delta A}]_{ssm}$, and 35 injections of 8 μL aliquots of ^{19}F-Man3 (4 mM) in the case of CVN^{mDB}, were performed at 2 min intervals from a 285 μL stirring syringe. Reverse ITC measurements were performed as follows: the ^{19}F-Man3 solution (50 μM) was placed in the calorimeter cell (ca. 1.44 mL active volume), stirred at 310 rpm, while $[CVN^{\Delta A}]_{ssm}$ or CVN^{mDB} solution were placed in the injector. 10 μL aliquots of 0.6 mM $[CVN^{\Delta A}]_{ssm}$ and 11 μL aliquots of 1 mM CVN^{mDB} were added at 2 min intervals from the 285 μL stirring syringe. A total of 28 injections were performed for $[CVN^{\Delta A}]_{ssm}$ and 25 injections for CVN^{mDB}. Binding isotherms were fit using the Origin 7.0 software by using a standard one-site model, to extract the apparent number of binding sites and affinity parameters. Values for the binding enthalpy, the apparent number of binding sites and affinities were obtained from the fit to the experimental data. Other thermodynamic parameters were calculated by using the standard expressions: $\Delta G = -RT \ln K_a$; $\Delta G = \Delta H - T\Delta S$.

^{19}F NMR spectroscopic competition binding assay: The binding affinities of Man3 for the CVN^{mDB} variant were quantified using a ^{19}F NMR-based competition assay. In this experiment, the non-labeled competitor ligand Man3 was titrated into a solution of ^{19}F-Man3 (250 μM) and CVN^{mDB} (25 μM) in sodium phosphate buffer (20 mM), pH 6.0, 0.01 % NaN_3, 90 % H_2O/10 % D_2O. A series of 1D-^{19}F NMR spectra were recorded at 280 K with ^{19}F-Man3/CVN^{mDB}/Man3 molar ratios of: 10:1:0, 10:1:0.25, 10:1:0.5, 10:1:0.75, and 10:1:1. The intensity increase of the free 1D NMR signal of ^{19}F-Man3 complexed with CVN^{mDB}, upon addition of the inhibitor (Man3), is proportional to the amount of non-labeled ligand (Man3) bound to CVN^{mDB}. The apparent dissociation constants k_d for Man3 binding to the Domain A of CVN^{mDB}, was obtained from best fitting the response curves with KaleidaGraph (Synergy Software, Reading, PA), by using a competitive binding Cheng–Prusoff equation (see Equation in Figure 7),[48] in which K_D^F is the dissociation constant of ^{19}F-Man3 binding to the Domain A of CVN^{mDB} (see above).

Acknowledgements

We thank Mike Delk for NMR spectroscopy technical support. This work was supported by a Science Foundation of Ireland Grant 08/IN.1/B2067 (to S.O.), funding from the EC (contract no. 26060, GlycoHIT; to H.J.G) and a National Institutes of Health Grant RO1GM080642 (to A.M.G.).

[1] *The Sugar Code. Fundamentals of glycosciences* (Ed.: H.-J. Gabius,), Wiley-VCH, Weinheim, Gemany, **2009**.

[2] S. Oscarson in *The Sugar Code. Fundamentals of glycosciences* (Ed.: H.-J. Gabius,), Wiley-VCH, Weinheim, Gemany, **2009**, pp. 31–51.

[3] H.-J. Gabius, S. André, J. Jiménez-Barbero, A. Romero, D. Solís, *Trends Biochem. Sci.* **2011**, *36*, 298–313.

[4] A. Imberty, Y. M. Chabre, R. Roy, *Chem. Eur. J.* **2008**, *14*, 7490–7499.

[5] J. Holgersson, A. Gustafsson, S. Gaunitz in *The Sugar Code. Fundamentals of glycosciences* (Ed.: H.-J. Gabius,), Wiley-VCH, Weinheim, Gemany, **2009**, pp. 31–51.

[6] M. Sperandio, C. A. Gleissner, K. Ley, *Immunol. Rev.* **2009**, *230*, 97–113.
[7] Y. M. Chabre, D. Giguere, B. Blanchard, J. Rodrigue, S. Rocheleau, M. Neault, S. Rauthu, A. Papadopoulos, A. A. Arnold, A. Imberty, R. Roy, *Chem. Eur. J.* **2011**, *17*, 6545–6562.
[8] H. Kaltner, H.-J. Gabius, *Histol. Histopathol.* **2012**, *27*, 397–416.
[9] G. M. Clore, A. M. Gronenborn, *J. Magn. Reson.* **1982**, *48*, 402–417.
[10] G. M. Clore, A. M. Gronenborn, *Protein Sci.* **1994**, *3*, 372–390.
[11] F. Ni, Y. Zhu, *J. Magn. Reson. Ser. B* **1994**, *103*, 180–184.
[12] V. Roldós, F. J. Canada, J. Jiménez-Barbero, *ChemBioChem* **2011**, *12*, 990–1005.
[13] C. Dalvit, *Prog. Nucl. Magn. Reson. Spectrosc.* **2007**, *51*, 243–271.
[14] A. Vulpetti, U. Hommel, G. Landrum, R. Lewis, C. Dalvit, *J. Am. Chem. Soc.* **2009**, *131*, 12949–12959.
[15] F. Millett, M. A. Raftery, *Biochem. Biophys. Res. Commun.* **1972**, *47*, 625–632.
[16] G. M. Alter, J. A. Magnuson, *Biochemistry* **1974**, *13*, 4038–4045.
[17] P. Midoux, J. P. Grivet, M. Monsigny, *FEBS Lett.* **1980**, *120*, 29–32.
[18] F. Jordan, H. Bahr, J. Patrick, P. W. Woo, *Arch. Biochem. Biophys.* **1981**, *207*, 81–86.
[19] R. U. Lemieux, *Chem. Soc. Rev.* **1989**, *18*, 347–374.
[20] D. Solis, A. Romero, H. Kaltner, H.-J. Gabius, T. Diaz-Maurino, *J. Biol. Chem.* **1996**, *271*, 12744–12748.
[21] D. Solís, A. Romero, M. Menédez, J. Jiménez-Barbero in *The Sugar Code. Fundamentals of glycosciences* (Ed.: H.-J. Gabius,), Wiley-VCH, Weinheim, Gemany, **2009**, pp. 233–245.
[22] T. Diercks, J. P. Ribeiro, F. J. Canada, S. André, J. Jiménez-Barbero, H.-J. Gabius, *Chem. Eur. J.* **2009**, *15*, 5666–5668.
[23] S. André, F. J. Cañada, T. C. Shiao, L. Largartera, *Eur. J. Org. Chem.* **2012**, 4354–4364.
[24] a) R. O'Brien, J. E. Ladbury, B. Z. Chowdry in *Protein-Ligand Interactions: hydrodynamics and calorimetry* (Eds.: S. E. Harding, B. Z. Chowdry), Oxford University Press, Oxford, **2001**, pp. 263–286; b) A. Brown, *Int. J. Mol. Sci.* **2009**, *10*, 3457–3477.
[25] C. A. Bewley, K. R. Gustafson, M. R. Boyd, D. G. Covell, A. Bax, G. M. Clore, A. M. Gronenborn, *Nat. Struct. Biol.* **1998**, *5*, 571–578.
[26] F. Yang, C. A. Bewley, J. M. Louis, K. R. Gustafson, M. R. Boyd, A. M. Gronenborn, G. M. Clore, A. Wlodawer, *J. Mol. Biol.* **1999**, *288*, 403–412.
[27] S. R. Shenoy, L. G. Barrientos, D. M. Ratner, B. R. O'Keefe, P. H. Seeberger, A. M. Gronenborn, M. R. Boyd, *Chem. Biol.* **2002**, *9*, 1109–1118.
[28] a) L. G. Barrientos, J. M. Louis, I. Botos, T. Mori, Z. Han, B. R. O'Keefe, M. R. Boyd, A. Wlodawer, A. M. Gronenborn, *Structure* **2002**, *10*, 673–686.
[29] A. J. Bolmstedt, B. R. O'Keefe, S. R. Shenoy, J. B. McMahon, M. R. Boyd, *Mol. Pharmacol.* **2001**, *59*, 949–954.
[30] L. G. Barrientos, A. M. Gronenborn, *Mini-Rev. Med. Chem.* **2005**, *5*, 21–31.
[31] C. A. Bewley, S. Kiyonaka, I. Hamachi, *J. Mol. Biol.* **2002**, *322*, 881–889.
[32] I. Botos, B. R. O'Keefe, S. R. Shenoy, L. K. Cartner, D. M. Ratner, P. H. Seeberger, M. R. Boyd, A. Wlodawer, *J. Biol. Chem.* **2002**, *277*, 34336–34342.
[33] C. Sandström, O. Berteau, E. Gemma, S. Oscarson, L. Kenne, A. M. Gronenborn, *Biochemistry* **2004**, *43*, 13926–13931.
[34] C. Sandström, B. Hakkarainen, E. Matei, A. Glinchert, M. Lahmann, S. Oscarson, L. Kenne, A. M. Gronenborn, *Biochemistry* **2008**, *47*, 3625–3635.
[35] L. G. Barrientos, E. Matei, F. Lasala, R. Delgado, A. M. Gronenborn, *Protein Eng. Des. Sel.* **2006**, *19*, 525–535.
[36] E. Matei, W. Furey, A. M. Gronenborn, *Structure* **2008**, *16*, 1183–1194.
[37] E. Matei, A. Zheng, W. Furey, J. Rose, C. Aiken, A. M. Gronenborn, *J. Biol. Chem.* **2010**, *285*, 13057–13065.
[38] C. Dalvit, A. Vulpetti, *ChemMedChem* **2011**, *6*, 104–114.
[39] C. Dalvit, A. Vulpetti, *ChemMedChem* **2012**, *7*, 262–272.
[40] A. Vulpetti, C. Dalvit, *Drug Discovery Today* **2012**, *17*, 890–897.
[41] R. Fromme, Z. Katiliene, B. Giomarelli, F. Bogani, J. Mc Mahon, T. Mori, P. Fromme, G. Ghirlanda, *Biochemistry* **2007**, *46*, 9199–9207.
[42] R. Perozzo, G. Folkers, L. Scapozza, *J. Recept. Signal Transduction* **2004**, *24*, 1–52.
[43] S. André, M. Lahmann, H.-J. Gabius, S. Oscarson, *Mol. Pharm.* **2010**, *7*, 2270–2279.
[44] F. Delaglio, S. Grzesiek, G. W. Vuister, G. Zhu, J. Pfeifer, A. Bax, *J. Biomol. NMR* **1995**, *6*, 277–293.
[45] B. A. Johnson, *Methods Mol. Biol.* **2004**, *278*, 313–352.
[46] G. Bodenhausen, G. Wagner, M. Rance, O. W. Soerensen, K. Wuethrich, R. R. Ernst, *J. Magn. Reson.* **1994**, *59*, 542–550.
[47] R. R. Ernst, G. Bodenhausen, A. Wokaun, *Principles of nuclear magnetic resonance in one and two dimensions*, Claredon Press, Oxford, **1987**.
[48] Y. Cheng, W. H. Prusoff, *Biochem. Pharmacol.* **1973**, *22*, 3099–3108.

Received: November 14, 2012
Revised: January 15, 2013
Published online: February 28, 2013

